DNA Crosslinked Alginate Hydrogels: Characterization, Microparticle Development and Applications in Forensic Science.

Amanda Orr[1], Paul Wilson[2], Theresa Stotesbury[3]*

[1] Environmental and Life Sciences Graduate Program (PhD), Trent University, 1600 West Bank Drive, Peterborough, ON, K9J 0G2

[2] Biology Department, Trent University, 1600 West Bank Drive, Peterborough, ON, K9J 0G2

[3] Faculty of Science, Forensic Science, Ontario Tech University, 2000 Simcoe Street North, Oshawa, ON, L1G 0C5

* Email: amandaorr@trentu.ca

KEYWORDS Forensic biomaterials; covalent crosslinking; tissue simulant; carbodiimide chemistry; chemical hydrogel; standard reference material; functional DNA

GRAPHICAL ABSTRACT Covalent crosslinking of alginate and ssDNA and general processing steps of hydrogel for forensic applications. Created with BioRender.com

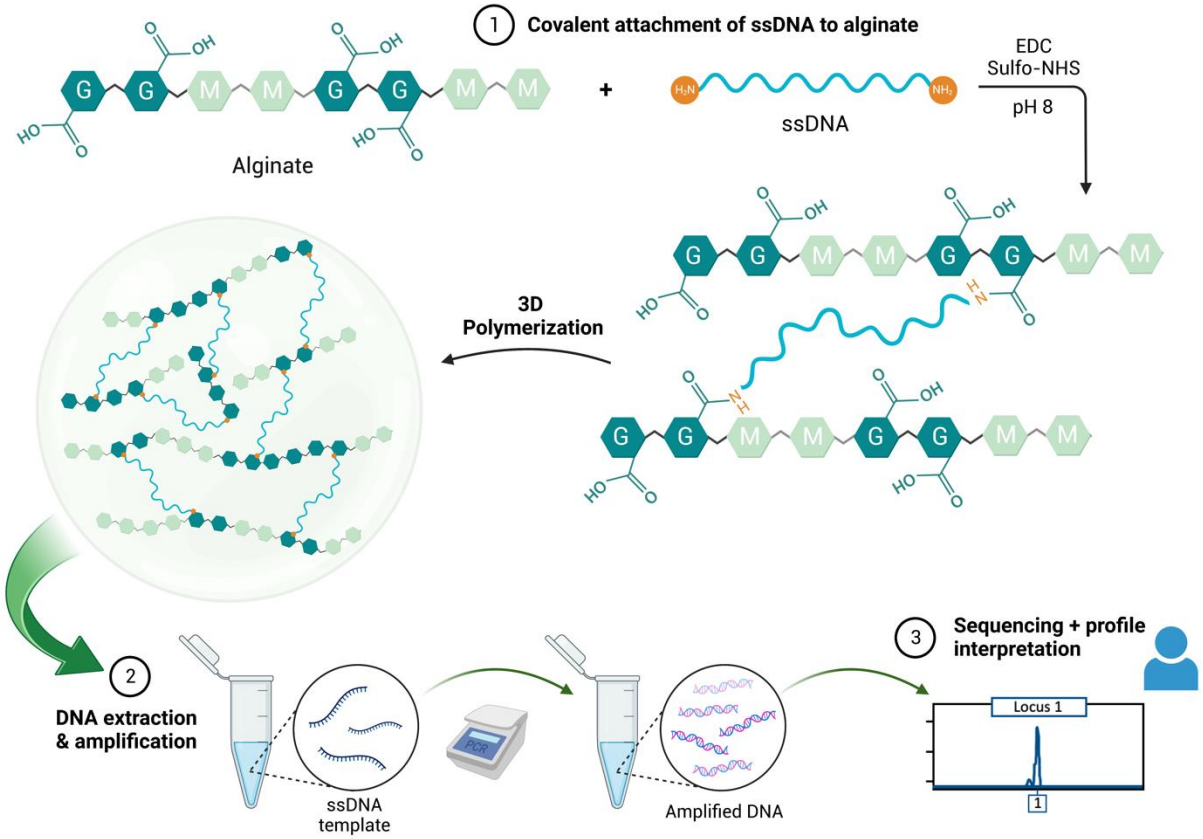

ABSTRACT

DNA-based hydrogels are attractive materials due to the integration of highly specific DNA sequences that can perform targeted functions for multiple fields. In this work we present a suite of materials with covalently bound ssDNA to an alginate-based hydrogel for targeted forensic applications. These crosslinked materials not only promote a more stable 3D polymeric network, but also achieve localization of functional ssDNA, a more desirable feature compared to previous DNA encapsulated versions. Specifically, dual amine terminated ssDNA (N-DNA-N) of three different concentrations was bound to alginate using carbodiimide chemistry. Rheological characterization showed that each DNA-crosslinked material forms similar structures, but the higher DNA concentration behaved like a dynamic viscoelastic material. FTIR analysis confirmed the formation of amide bonds, indicative of successful crosslinking between the N-DNA-N and alginate. SEM visualization also showed that each material had distinct topographies, where the covalent crosslinked alginate-DNA materials had more ordered particles and networked structures. We also investigated ssDNA with three different amine functionalities to understand the amine reactivity, which revealed that the N-DNA-N attaches primarily from the terminal primary amines on the DNA strands. From this, microparticles (MPs) using the DNA-crosslinked materials were developed, and the particle morphology and sizes were measured. It was determined that MPs made using DNA-crosslinked materials had larger particle diameters compared to the non-DNA controls, which is ideal for the generation of white blood cell (WBC) mimetics in forensic materials. In addition, these MPs could be successfully processed in a relevant forensic scenario through extraction, amplification, and genotyping, demonstrating the functionality of these materials to forensic blood simulants.

1. Introduction:

Alginate-based hydrogels have continually been developed in the areas of bioengineering, biomedicine, and the food industry owing to the many benefits of alginate such as biodegradability, printability, and low toxicity[1–5]. Not only is alginate a desirable polymer for these applications given its biocompatibility and mechanical similarities to the extracellular matrix (ECM)[6], but also due to its versatile crosslinking potential. Covalent crosslinking of alginate can be used to design chemically modified hydrogels (chemical gels) with targeted functions, mechanical, and/or chemical capabilities. Alginate is comprised of repeating blocks of β-D-mannuronate (M) and α-L-guluronate (G), each containing carboxyl (COOH) functional groups. The COOH moieties are one of the main sources of covalent crosslinking of alginate[7], where typical crosslinking can be achieved through incorporation of photoionizable groups[8–10], click chemistry[11], carbodiimide chemistry[12,13], or through esterification reactions with alcohol- or alkyl halide-functionalized groups[14]. Other types of crosslinking include ionic and pH-induced crosslinking, but are often not used in biomaterial development due to properties such as gel instability and lack of stiffness when compared to covalently crosslinked materials[15,16]. Recent work has even demonstrated the potential of hydrogels to be developed without the use of traditional crosslinkers, where hydrogel polymerization is controlled via physical forces such as hydrogen bonding and electrostatic interactions while retaining similar properties to crosslinked hydrogels[17].

Hydrogels can incorporate a variety of crosslinkers including deoxyribonucleic acids (DNA). DNA-based hydrogels are an emerging and attractive option for polymer materials primarily due to the predictable and base-specific binding of DNA[18]. Further, DNA integration into hydrogels procures additional benefits such as controlled biodegradation, spatial control, and stimuli responsive behaviour[18,19]. DNA-containing hydrogels are extremely versatile and programmable materials that make these hydrogels useful in host recognition or controlled transfection of DNA[15], biosensensing[20], and drug delivery applications[19,21]. Commonly, these materials incorporate aptamers in the hydrogel matrix; which are short single stranded ligands with high specificity for a given target molecule(s)[22]. The aptamers can be used as either single stranded crosslinkers, or can be hybridized with its complementary strand to form crosslinked hydrogels[18,22]. Most often, the aptamers are constructed through functionalization or decoration of polymers[23] that primarily provide functional properties within a hydrogel[19]. However, the DNA can be included for both mechanical and functional purposes, where the three-dimensional (3D) crosslinked networks are formed through hybridization of two complementary immobilized single stranded DNA (ssDNA). One example of a crosslinked 3D hydrogel using alginate and DNA was developed for controlled release of fluorescein isothiocyanate-dextran (FITC-dextran) using an egg white lysozyme aptamer[24]. By including the aptamer hydrogel, targeted degradation occurred in the presence of the specific lysozyme, thus releasing the encapsulated drug simultaneously. Beyond aptamer-based DNA hydrogels, various forms of DNA can be integrated into the polymer network, including

X- or Y-DNA/nanostars, i-Motifs, DNAzymes, and Guanine-quadruplexes using a variety of modification strategies[19,25,26]. For example, using X- and Y-shaped DNA, hydrogels can be easily tuned to possess properties such as self-healing[27], controlled stiffness and degradation[28], all while produced under physiological and non-toxic conditions. G-quadruplexes and i-motifs can be used to achieve hydrogels with photo-responsiveness and shape-memory functionalities[29,30], and DNAzymes can be effective in the colorimetric detection of hydrogen peroxide (H_2O_2) down to 1.0 μm[31].

While DNA-crosslinked hydrogels have been investigated previously, the included sequence is usually some form of an aptamer, and these materials typically focus on other polymer bases such as polyacrylamide[18,20,32,33], polyethylene glycol[18,34], or even DNA itself[35,36], but infrequently alginate. In addition, the design of these materials is typically tailored for therapeutic or biosensing applications in biomedicine and bioengineering. While these applications are advantageous, biofunctional materials – such as DNA-based hydrogels, have clear relevance to other fields such as forensic science. In forensic science, DNA-based hydrogels can be used for the detection of a variety of analytes drugs, metabolites, and identification of biological evidence[37]; and for imaging of latent fingerprints[38]. Beyond these applications, and the focus of this research, is the development of functional tissue mimetics or standard reference materials with controlled hydrogel properties. These materials can assist in training and understanding the complex degradation mechanisms experienced by biological tissues in crime scene scenarios.

The present work focused on the 3D crosslinking of alginate and ssDNA that can be amplified with human CODIS loci primers[39,40]. The purpose of this research was to characterize the covalent crosslinking between alginate and dual amine ssDNA to expand on our previous research with ionically crosslinked DNA-encapsulated alginate hydrogels (CATGs)[41]. Here, we explore covalent crosslinking with DNA strands of similar size; where the dual amine-terminated 98-base ssDNA was covalently crosslinked to alginate using carbodiimide chemistry. Covalently crosslinked alginate-DNA hydrogels are desirable to localize DNA binding in the alginate and develop more stable hydrogels, which have significant forensic applications

2. Experimental Section

2.1 *Materials*

1% w/v alginate (low viscosity, Sigma, Oakville, ON) was dissolved in MES buffer (0.05 M, pH 6.0) and allowed to mix overnight at room temperature (22°C ± 2°C). 1-ethyl-3-(3-dimethylaminopropyl) carbodiimide•HCl (EDC, BioShop, Burlington, ON) and *N*-hydroxysuccimide (Sulfo-NHS, ThermoFisher, Mississauga, ON) were used as received. The ssDNA crosslinker was purchased from Integrated DNA Technologies (Toronto, ON) and reconstituted in UltraPure™ water to create a 100 µM stock solution. The crosslinker was a 98-base ssDNA[41] with primary amine groups ($NH_2 - R$) on both the 5' and 3' ends (N-DNA-N). Various amine modified ssDNA were also investigated, including: i) primary amines on both the 5' and 3' ends – "N-DNA-N" (AXD2N), ii) primary amine on the 5' end – "N-DNA" (AXD1N) and iii) no terminal amines – "DNA" (AXD0N) (Table 1).

2.2 *Crosslinking Scheme*

Each crosslinking reaction had a total volume of 5 mL. First, 1% w/v alginate (MES) was added to individual vials on a stir plate, and EDC (261 µmol) and Sulfo-NHS (65 µmol) were added and allowed to react for 20 minutes at room temperature (22°C ± 2°C). 100 µL of NaOH (1 M) was added to raise the pH to 8 before the addition of the ssDNA (N-DNA-N, N-DNA or DNA). Various concentrations of the DNA crosslinker were added (0.01, 0.025 and 0.05 µmol = 0.02, 0.05 and 0.1 µmol amines, respectively) to assess the effects of crosslinking on the materials. The general reaction scheme is shown below (Scheme 1). The samples were allowed to react for 24 hours and EDC/Sulfo-NHS removal was completed using Amicon Ultra 30K MWCO filtration units. Three filtration/wash steps were performed: i) filtration step (1000 x g, 30 minutes), ii) wash step 1 (1000 x g, 15 minutes), and iii) wash step 2 (1000 x g, 15 minutes). 1 mL of MilliQ® water was added to each sample before each of the wash steps. In total, nine materials were formed: seven different materials with the carbodiimide crosslinkers present, as well as two controls without crosslinkers (Table 1).

Scheme 1. Covalent attachment of dual amine-terminated ssDNA to alginate polymer. Created with BioRender.com

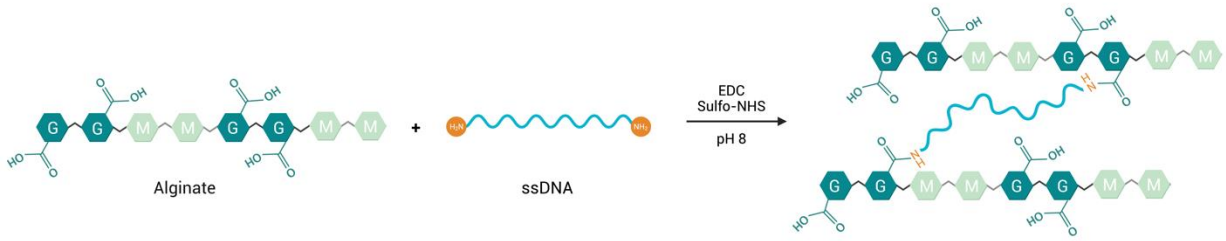

Table 1: Outline of crosslinking reactions. The presence of "X" indicates that the covalent crosslinkers EDC and Sulfo-NHS were added to reaction, whereas "P" indicates the DNA was mixed with alginate without EDC/Sulfo-NHS. Identification in square brackets represents the classification with the addition of Ca^{2+}.

Main Crosslinking [+ Ca^{2+}]	Material	EDC (μmol)	Sulfo-NHS (μmol)	ssDNA Structure	ssDNA Concentration (nmol)	pH
Covalent [Dual]	AX_0	261	65	--	--	8
	AXD10	261	65	N-DNA-N	10	
	AXD25	261	65	N-DNA-N	25	
	AXD50	261	65	N-DNA-N	50	
	AXD0N	261	65	DNA	50	8
	AXD1N	261	65	N-DNA	50	
	AXD2N	261	65	N-DNA-N	50	
Non-Covalent [Ionic]	A_0	--	--		--	8
	APD50	--	--		50	

2.3 *Materials Characterization*

2.3.1 *Rheology*

For the rheological characterization, samples were made to be dual crosslinked (4:1 volume ratio alginate:calcium (50 mM $CaCl_2$); where "alginate" in this case refers to the final material – or "material" – from Table 1). Rheological assessments were conducted using a Discovery HR20 stress-controlled rheometer with an advanced Peltier plate and solvent trap system (TA Instruments). All rheological tests were conducted at 22°C using a 40 mm parallel plate geometry with Millipore water in the solvent trap and a 500 μm gap. Oscillation amplitude sweeps and frequency sweeps were preformed between strains of 0.01-150% and frequencies of 0.05-200 rad/s, respectively. The frequency sweeps were conducted at a strain of 2%.

2.3.2 *Fourier Transform Infrared Spectroscopy (FTIR)*

FTIR and SEM analyses were performed using both the DNA crosslinked materials and controls, both with and without the addition of Ca^{2+}. For the FTIR characterization, 1 mL disposable transfer pipettes were used to place three drops of each material into individual Petri dishes and were allowed to dry. The dried films were placed directly on the FTIR crystal for analysis. FTIR measurements were conducted using a Thermo Fisher Nicolet 380 FTIR spectrometer in absorbance mode (ATR) between wavenumbers of 4000-500 cm^{-1} with a total of 32 scans.

2.3.3 *Scanning Electron Microscopy (SEM)*

SEM analyses were used for morphological characterization of the materials, using a Hitachi's FlexSEM 1000 Scanning Electron Microscope. The materials were allowed to air dry on stainless

steel stubs, and analyzed at 5 kV. Images were magnified at 500 (100 µm scale), 1K (50 µm scale), and 2K (20 µm scale) SE, and certain images were analyzed at 4K SE (10 µm scale).

2.3.4 Thermogravimetric Analysis (TGA)

TGA was used for materials characterization of the different amine variation ssDNA materials, where only dual crosslinked materials were investigated. For this, a TA Instrument SDT Q600 thermal analyzer was used. The dual crosslinked materials were freeze-dried for 24 hours prior to TGA analysis and the freeze-dried materials (8 – 12 mg) were analyzed between 25°C to 800°C, with a heating rate of 10°C/min, and under Argon gas (50 mL/min).

2.4 *Electrospray Ionization Optimization & Microparticle Generation*

Before microparticle (MP) development with the crosslinked materials, an optimization experiment was first conducted using alginate dissolved in water, Alg(H_2O), to understand the effects of concentration, voltage (V), spraying distance (*d*), and flow rate (Q) on MP formation. For the purposes of this research, the optimized conditions were found to be: 2.5% w/v alginate + 0.5% v/v Tween 20 at a flow rate of 2 µL/min, with 10 kV applied to the needle tip that was 4 cm from the $CaCl_2$ collection bath (7.35 wt/v%). Following optimization, MPs were created using the 2.5% w/v alginate dissolved in MES buffer, Alg(MES), a crosslinking control (AX_0) and two DNA crosslinked materials – a low concentration of DNA (AXD10) and a high concentration (AXD50). Each crosslinked material was made using the same conditions as Section 2.2, with the exception that 2.5% w/v alginate was used instead of 1% w/v. The DNA used in the crosslinking reactions was the dual amine terminated 98-base strand (N-DNA-N).

The electrosprayed MPs were washed three times with MilliQ® water before visualizing on an EVOS FL Auto microscope (Life Technologies) under 20x and 40x magnification in brightfield mode. Once imaged, the images were imported into Fiji (Image J, 2.3.0/1.53q), scaled, and the particle diameters were manually measured using the "Measure" tool. RStudio (2022.07.1) was used to statistically compare the respective particle diameters using a student's t-test, and generate the particle size distributions.

2.5 DNA extraction and amplification of the MPs

Finally, the washed MPs underwent an extraction and amplification process, similar to a method used in our previous work with CATGs[41]. Specifically, the MP solutions were first inverted to ensure homogenous distribution of MPs, and 100 µL was added to 450 µL of gel dissolving buffer (Monarch® DNA Gel Extraction Kit, New England Biolabs). The MPs were incubated at 52°C and 500 rpm for 20 minutes (Eppendorf ThermoMixer F1.5), and the manufacturer's protocol was followed as suggested hereafter. The DNA was eluted with 20 µL of Invitrogen™ UltraPure water (ThermoFisher Scientific). 2 µL of the extracted DNA was added to a 10 µL PCR reaction (95°C for

10 minutes; 94°C for 30 seconds; 53°C for 1 minute; 72°C for 1 min; repeated for a total of 30 times with a final step of 65°C for 15 minutes). A 1:50 dilution of the amplified product was genotyped using an ABI 3730 DNA Analyzer with a GeneScan 500 ROX size standard.

3. Results and Discussion

3.1 *Rheology*

The rheological analyses show that overall, the ionically crosslinked samples have much higher storage (G') and loss moduli (G'') compared to the dual crosslinked counterparts (Figure 1). This is unlike other studies with dual crosslinking[8,10,42]; however, there are two likely explanations for the lower moduli values in the dual crosslinked samples. First, the egg box model of Ca^{2+}-Alg hydrogels leads to tighter junctions, and therefore stiffer gels compared to the hydrogels crosslinked with elastic and larger ssDNA. Further, if alginate is bound to either N-DNA-N, or in the case of the Ca-AX_0, likely bound to Sulfo-NHS (see Section 3.2), there are less available COO^- groups to participate in Ca^{2+} coordination, leading to softer materials. Additionally, the DNA used in this research is typically larger than the length of DNA incorporated into other hydrogels through 3D crosslinking or functionalization. For example, aptamers can typically range between 20-60 nucleotides[43], but a majority of works that include functionalized ssDNA is less than 40 nucleotides. Further, the attachment of ssDNA is usually bound by a single end, where the 3D hydrogel formation is achieved through either hybridization of complementary sequences of bound strands[24] or through hybridization of another unbound complementary strand[44]. Using similar attachment strategies to the one used in our research (ssDNA immobilized by both the 5' and 3' ends), Murakami et al[20] used 29-base amine-terminated ssDNA to investigate the ability of the DNA-crosslinked hydrogel to shrink or swell when bound to complimentary strands, but did not investigate the rheological profile of these materials. Pan et al[45] investigated the effect of rigid and flexible DNA strands on the hydrogel rheology and found that flexible chains can lead to better stability and stretchability, although Jiang and coauthors have shown that longer DNA strands can lead to softer gels[46]. In our hydrogels, we observed the latter, where the long ssDNA incorporated into our hydrogels leads to very flexible, and soft gel characteristics. Because of this, we do not see linear trends in our moduli values, where the G' should be much larger than G'' as the DNA concentration (and theoretically number of crosslinks) is increased.

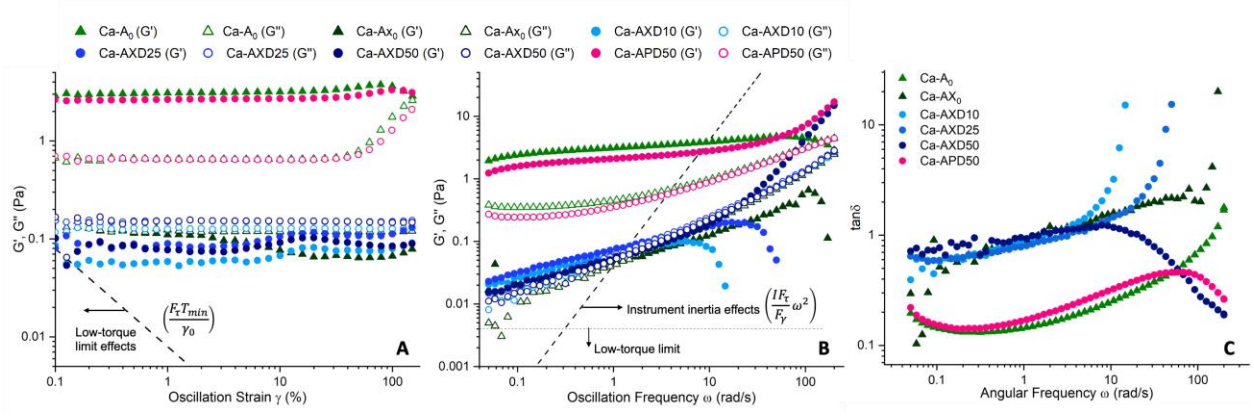

Figure 1. Amplitude sweeps (A), frequency sweeps (B) and tanδ (C) for 6 different ionic and dual crosslinked materials. The filled in symbols represent the Storage Modulus (G') and the corresponding non-filled symbols

are the Loss Modulus (G'') for a given sample. Overlayed lines represent potential inertial limits based on low torque and instrument inertial effects as outlined by Ewoldt[47]. Limits are based on geometry-specific stress constant (F_τ), minimum torque of instrument (T_{min}), minimum strain (γ_0), instrument inertia (I), geometry-specific strain constant (F_γ) and frequency (ω).

In the amplitude sweeps, the dual crosslinked materials each had G''>G' indicating the formation of viscous materials instead of elastic (Figure 1A). Each DNA crosslinked material showed similar curve characteristics, demonstrating similar structural formations, and had distinct behaviour in the amplitude sweeps as demonstrated in another study[48]. The DNA exhibits strain stiffening at the higher oscillation strains, due to its elastic nature. This behaviour is different from the Ca-AX_0 sample as the material has a smaller linear viscoelastic region, and exhibits more of a structural breakdown in the same strain range (Figure 1A).

In the frequency sweeps, the Ca-AXD50 was the only material of the dual crosslinked materials that did not exhibit structural breakdown at higher frequencies (Figure 1B). This breakdown was concentration-dependant, where Ca-AXD10 deforms first (7.9 rad/s), followed by Ca-AXD25 (23.2 rad/s), and then Ca-AX_0 (107.7 rad/s), where the Ca-AXD50 does not show structural breakdown (Figure 1B). In the high frequency region (>100 rad/s), Ca-AXD50 behaves like a viscoelastic material[49], where G'>G'', and the material shows high frequency dependence. Frequency dependence can indicate dynamic gels[50], which is likely the case. Besiri et al[51] have shown that higher frequencies can lead to increased distribution of Ca^{2+} during *in situ* assessments of Ca-alginate crosslinking. These higher frequencies can theoretically disrupt the coordinated Ca^{2+} ions in the dual crosslinked materials, causing structural deformation. Consequently, the Ca-AXD50, which has more covalent crosslinks, can then withstand the higher frequencies despite the reorganization of the Ca^{2+} ions. The Ca-AXD50 also showed less frequency dependence at lower frequencies in the tanδ (Figure 1C), indicating a more relatively stiff material compared to the other dual crosslinked counterparts. It should be noted that other work has suggested the influence of inertial effects in the high frequency range of low viscosity materials which can be misinterpreted as structural response[47]. When the inertial limits are overlayed over the rheological data (Figure 1) the high frequency region could be influenced by inertial effects, although replicate analyses suggest this is a true material behaviour (Figure 1, Figure 4).

Interestingly, even though we see a distinct structural difference in the Ca-AXD50 in the frequency sweep, there was not a large difference between the Ca-AXD50 and Ca-AXD25 in the amplitude sweep. In fact, the Ca-AXD25 shows a higher G' compared to the Ca-AXD50. This observation could be due to the Ca^{2+} interactions offsetting the extra DNA crosslinking occurring in the Ca-AXD50; where less DNA crosslinks in the Ca-AXD25 means that more Ca^{2+} can interact with the COO^- groups, leading to higher G' overall.

3.2 FTIR Spectroscopy

The FTIR spectra showed similar trends to the rheology analyses, especially regarding the AXD50 sample. The main comparison is shown between the DNA-crosslinked samples (AXD10, AXD25, and AXD50) and controls (AX_0, A_0, APD50) (Figure 2). The control materials were included to directly assess the effects of the covalent crosslinkers (AX_0) as well as the presence of ssDNA on the hydrogel structure (APD50).

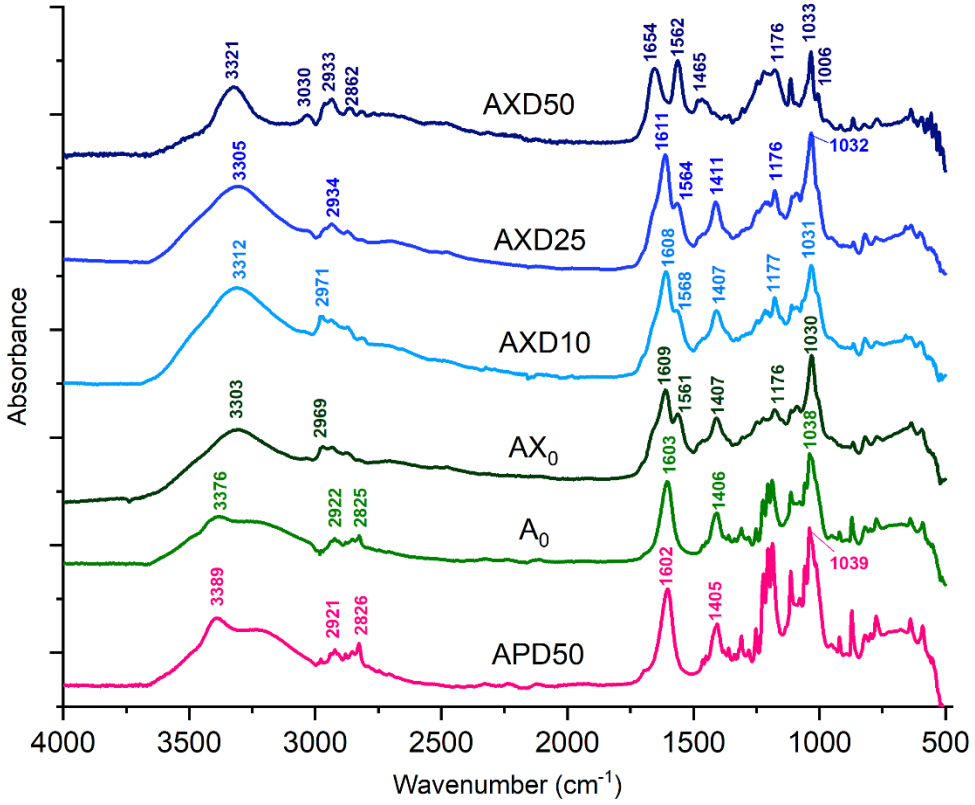

Figure 2. FTIR spectra for six different alginate materials. Materials AX_0, AXD10, AXD25, and AXD50 were covalently crosslinked using EDC/Sulfo-NHS only (no Ca^{2+}); and samples A_0 and APD50 were mixed without the addition of EDC/NHS or Ca^{2+}.

Alginate was observed to have characteristic peaks at 1603 and 1406 cm^{-1}, which corresponds to the COO^- moieties of the M and G blocks, specifically the symmetrical stretching of the carbonyl groups (C=O) at 1603 cm^{-1} and asymmetrical stretching (C-OH) at 1406 cm^{-1} [52]. In the presence of EDC/Sulfo-NHS, the 1603 cm^{-1} peak is split into two peaks at 1609 and 1561 cm^{-1}, which is likely due to residual C=O in solution from Sulfo-NHS. This is also supported given that S=O stretching can be seen only in the covalent materials at 1176 cm^{-1}.

In the AXD50 material, there is an even further red shift in the split peaks to 1654 cm^{-1}, attributed to the amide I bond formation. There is also an additional simultaneous loss of the 1407 cm^{-1} peak. Both changes indicate the loss of COO^- groups, which occurs during amide bond formation from

N-DNA-N binding to the alginate (Scheme 1). Other indicators of amide bond formation are observed in the increased absorbance of the peak at 1562 cm^{-1}, likely due to the N-H deformation of amide II[53]. There is also a more distinct peak at 3321 cm^{-1}, which is reasoned to be caused by N-H stretching of the amide A bond[53]. The addition of N-DNA-N in the alginate material without crosslinkers (APD50) shows relatively no change to the COO^- groups. This indicates that the presence of DNA alone is not leading to the amide bond detection observed in the DNA-crosslinked materials, which naturally exist in three of the four DNA bases. An interesting note is the shift of the asymmetrical stretch of the -COO^- to a higher wavenumber in the in the APD50 sample from 1407 cm^{-1} to 1410 cm^{-1}. This could be due to the interaction of the N-DNA-N ions with the negatively charged alginate, although another study showed a shift to higher numbers without Ca^{2+} interaction[54].

In both the FTIR and SEM assessments, the calcium-crosslinked samples (ionic, dual) showed less distinct differences overall (Supporting Information), especially between covalently crosslinked samples. This is likely the result of the calcium ionic crosslinks masking any underlying covalent linkages between DNA and alginate, as mentioned previously. It should be noted that even though materials made with the addition of calcium showed less distinct differences in the SEM and IR assessments, the rheological assessments did observe distinct differences, largely as the technique can directly probe the viscoelastic properties of materials on a more sensitive molecular level.

3.3 SEM

Analyses with SEM showed that the DNA-crosslinked materials had more order and structured surfaces compared to encapsulated N-DNA-N (APD50) and the non-DNA containing materials (AX_0, A_0) (Figure 3). Both the A_0 (Figure 3, A and B) and AX_0 (Figure 3, C and D) materials had relatively smooth and pitted surface morphologies compared to any of the DNA-containing materials. The DNA-crosslinked materials exhibited varying surface morphologies, signifying more structured and complex materials (Figure 3, E-J). Compared to the DNA-crosslinked materials, the APD50 sample displayed a more porous structure, with a less structured fibrous surface (Figure 3, K and L). This contrasts the covalently crosslinked counterpart, where more circular aggregations were observed with more apparent order (Figure 3, J) and intricate networks (Figure 3, I).

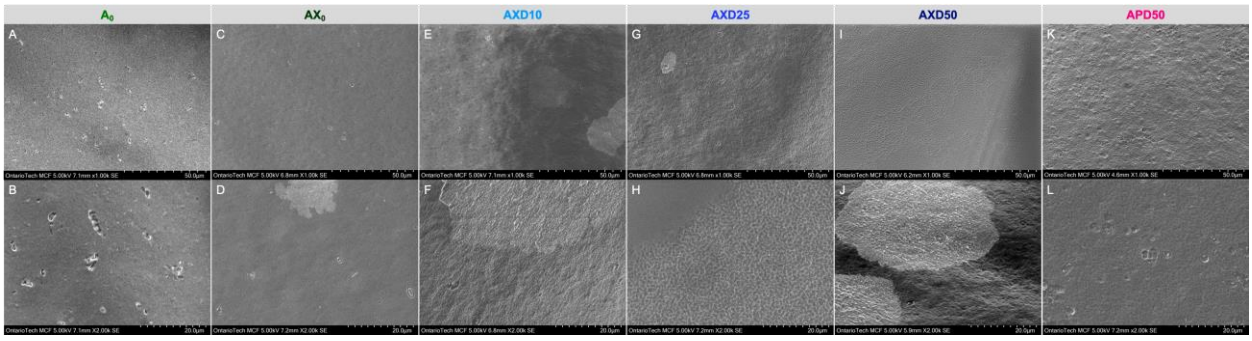

Figure 3: SEM images of six different materials with/without crosslinkers and with/without N-DNA-N. Samples from left to right are: A_0, AX_0, AXD10, AXD25, AXD50, and APD50. The first row shows magnification at approximately x1000 (50 µm scale intervals), and the second row is x2000 (20 µm intervals).

As mentioned previously, the calcium crosslinked samples (dual or ionic) demonstrated less distinct surface morphologies between samples, but still showed general material differences including more bulbous surfaces in the non-crosslinked controls and particle shape differences between the DNA-crosslinked materials compared to the alginate controls (see Supporting Information).

3.4 Influence of ssDNA Structure

The different ssDNA structures used in the crosslinking reaction (N-DNA-N, N-DNA, DNA) did appear to influence the overall material properties. When assessed with rheology, materials crosslinked with either dual ended amine ssDNA (Ca-AXD2N) or single amine ssDNA (Ca-AXD1N) did not exhibit any structural breakdown at high frequencies, similar to Ca-AXD50, and was unlike the alginate material covalently crosslinked with DNA without any terminal amines (Ca-AXD0N) (Figure 4). The replicate dual amine DNA crosslinked material (Ca-AXD2N) demonstrated more of a linear viscoelastic region (LVR) in the amplitude sweep (Figure 4A) compared to the first reaction (Ca-AXD50, Figure 1A). When ssDNA without any terminal amines was reacted in a covalent crosslinking reaction (Ca-AXD0N), the material has a lower G' compared to the materials crosslinked with DNA that contain terminal amines (Figure 4A). Interestingly, the Ca-AXD0N material behaves differently than both encapsulated ssDNA (Ca-APD50, Figure 1A) and the alginate covalent controls (Ca-AX_0, Figure 1A, Figure 2A), indicating a unique material influenced by the lack of terminal amines. Further, the FTIR analyses detected no amide bonds the AXD0N material (Figure 5), suggesting that the DNA without terminal amines is not covalently attaching to the alginate as the AXD2N and AXD1N do. Without chemically attaching to the alginate backbone directly, the EDC can still react with the phosphate backbone of the DNA[55], which could be causing nonspecific reactions between DNA molecules and therefore a structurally weak material hydrogel. This is also supported through the SEM, where the AXD0N material appears more porous similar to the AX_0 material, but is unlike the AXD1N and AXD2N have more smooth and structured surfaces (Figure 5 A-H).

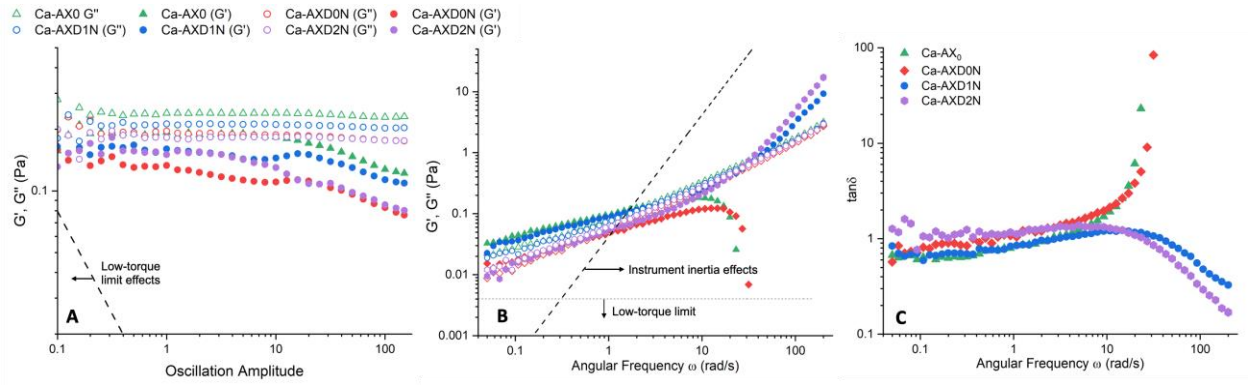

Figure 4. Amplitude sweeps (A) and frequency sweeps (B) and tanδ (C) for 4 ssDNA with varying amine reactivities: no DNA (Ca-AX_0), ssDNA with no terminal amines (Ca-AXD0N), one terminal amine (Ca-AXD1N), and two terminal amines (Ca-AXD2N) covalently crosslinked with alginate. The samples were made to be dual crosslinked with Ca^{2+}. The filled in symbols represent the Storage Modulus (G') and the corresponding non-filled symbols are the Loss Modulus (G'') for a given sample.

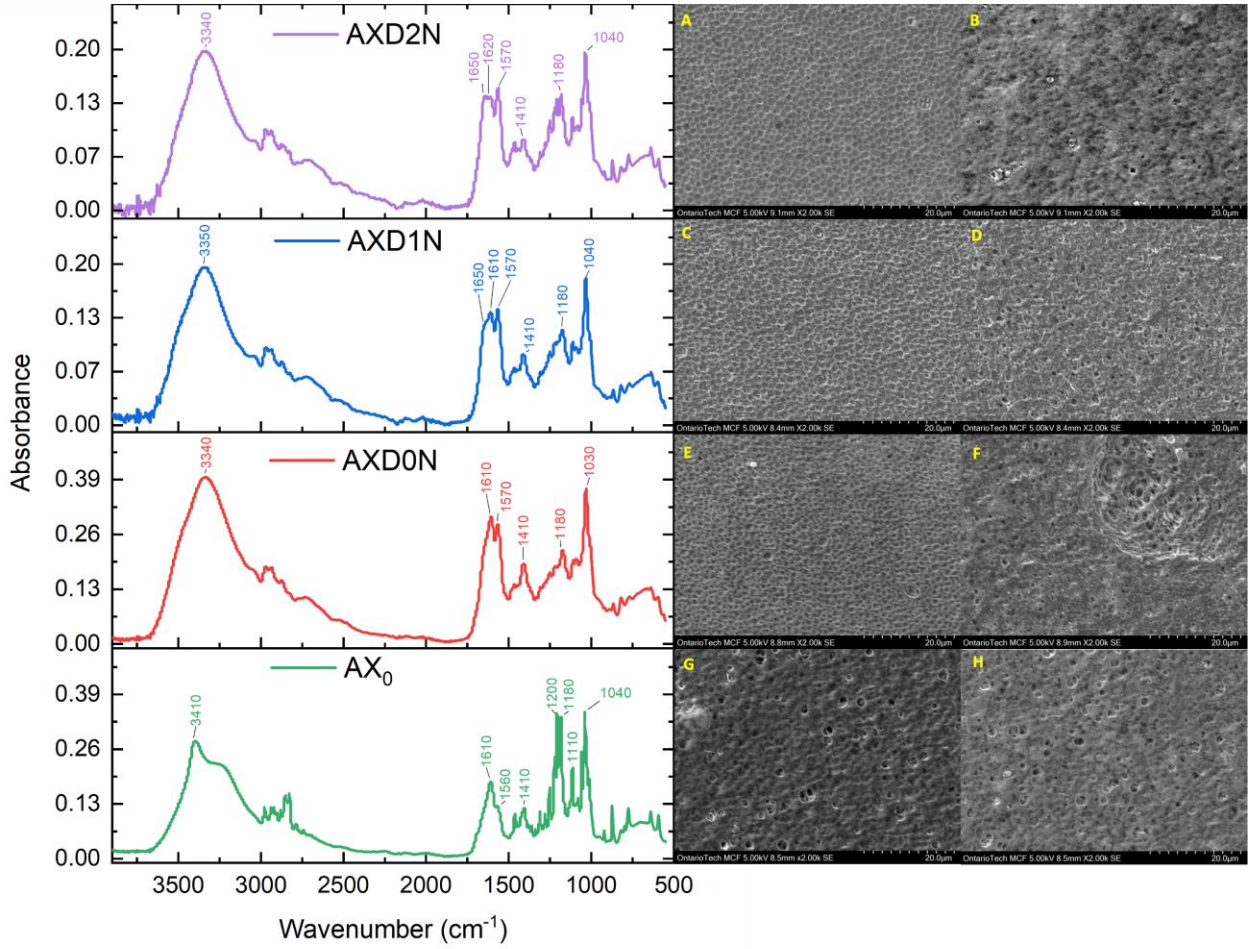

Figure 5. FTIR spectra (left) 4 different alginate materials crosslinked with no DNA (AX_0), ssDNA with no terminal amines (AXD0N), ssDNA with one terminal amine (AXD1N), and ssDNA with two terminal amines (AXD2N).

Images on the right show the corresponding SEM images of each material. Two SEM images are included to show the variation in surface morphologies.

Finally, TGA denoted overall similar degradation profiles (Figure 6), with slight variation during each degradation event. Ayouch et al[56] indicate that alginate-based materials can undergo three degradation events; between 30-150°C (water desorption), 200-300°C (decomposition of carbon in alginate backbone and formation of sodium carbonate – $NaCO_3$), and 600-700°C (two-stage breakdown of $NaCO_3$). Our TGA analyses showed similar degradation characteristics in the materials, with more distinct material differences shown at higher temperatures. The Ca-AXD2N material had the least relative amount of weight loss (74.37%) compared to Ca-AXD1N (78.16%), Ca-AXD0N (77.38%) and Ca-AX_0 (82.49%). At the higher temperatures (over 600°C), the alginate control (Ca-AX_0) is more easily degraded compared to the other materials, which is likely due to the strong molecular networks of the DNA-crosslinked materials[57], and explains why the Ca-AXD2N has more residual material.

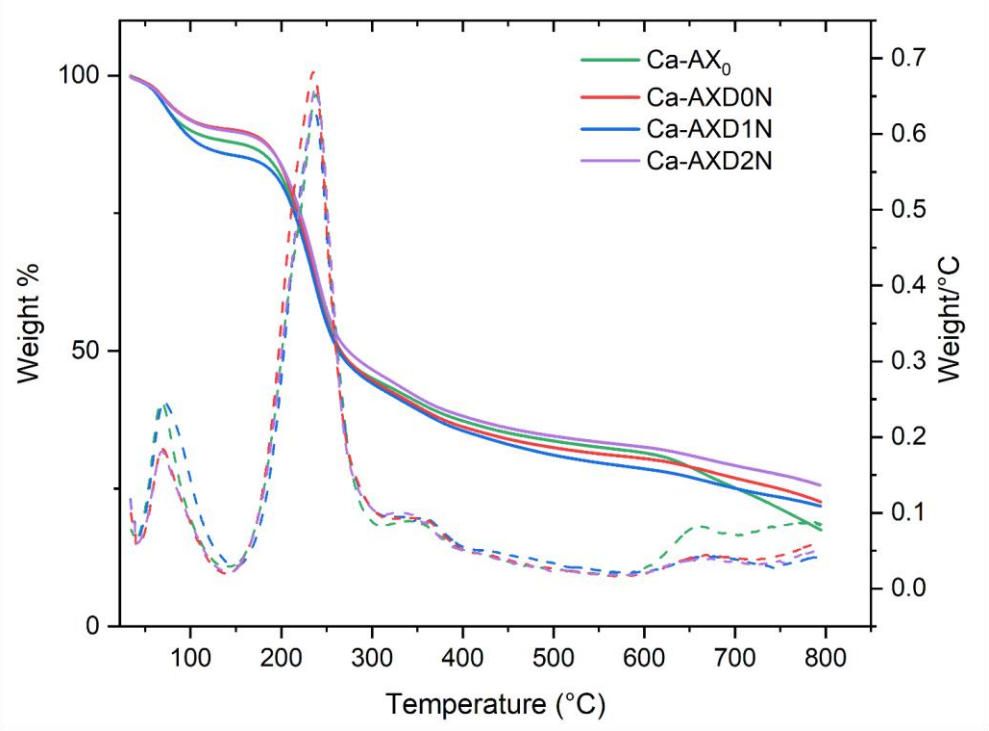

Figure 6: TGA curves of four different dual crosslinked alginate materials covalently crosslinked with no DNA (Ca-AX_0), ssDNA with no terminal amines (Ca-AXD0N), ssDNA with one terminal amine (Ca-AXD1N), and ssDNA with two terminal amines (Ca-AXD2N). Samples were made to be dual crosslinked with Ca^{2+}. The dashed curves represent Weight/°C, while the solid curves are the Weight % at each temperature

Together, the analyses signify that the amine modification of ssDNA at either one or both terminal ends leads to the immobilization of DNA to alginate. The ability to covalently attach the

DNA by either one end or both ends is particularly beneficial as it allows for many applications of the hydrogel materials. Specifically, the development of microparticles (MPs) using DNA-crosslinked alginate is of particular interest and is discussed in the next section.

3.5 *Microparticle Generation & Applications*

Human reference standards with the hydrogels can be developed in many forms, but one valuable application is the development of forensic blood simulants that have both relevant fluid properties and genetic capabilities similar to human blood[58,59]. To accomplish this, the covalently crosslinked alginate and ssDNA hydrogels were used to develop microparticles (MPs) of relevant white blood cell (WBC) size(s). MPs can be effectively generated through electrospray ionization (ESI), where the covalent crosslinked alginate-DNA is extruded through an electrified needle into a calcium bath with a counter electrode. The overall MP size and morphology is influenced by many factors[60], but the covalent materials must be able to coordinate effectively with Ca^{2+} to achieve relevant MPs, especially for our applications.

The MPs assessed in this work included those derived from Alg(MES), AX_0, AXD10 and AXD50, all with 2.5% w/v alginate. The 2.5% Alg(MES) was used as a control to compare to materials that had undergone the conditions of a crosslinking reaction (AX_0) and a crosslinking reaction with both low (AXD10) and high (AXD50) ssDNA concentrations. Tween 20 was added to the materials as a non-ionic co-solvent to lower the surface tension of the materials[61,62], which allowed for a more stable Taylor cone and more homogenous particle distributions. The two non-DNA materials (2.5% Alg(MES) and AX_0) had similar average particle diameters ($p = 0.78$), and were smaller than the DNA-crosslinked MPs (Figure 7). The AXD10 material had MPs that were statistically different from both 2.5% Alg(MES) ($p = 0.0003$) and AX_0 ($p = 0.0004$). Similarly, the AXD50 was also statistically different from both 2.5% Alg(MES) ($p = 6.81 \times 10^{-5}$) and AX_0 ($p = 9.91 \times 10^{-5}$). Interestingly, it appears that by crosslinking alginate with DNA, the MPs are larger than MPs electrosprayed without DNA. This is true irrespective of the concentration of DNA attached to alginate, as both AXD10 and AXD50 had similar average particle sizes ($p = 0.68$). This finding is appropriate for the development of human blood simulants, since WBCs are typically larger than red blood cells (RBCs) naturally.

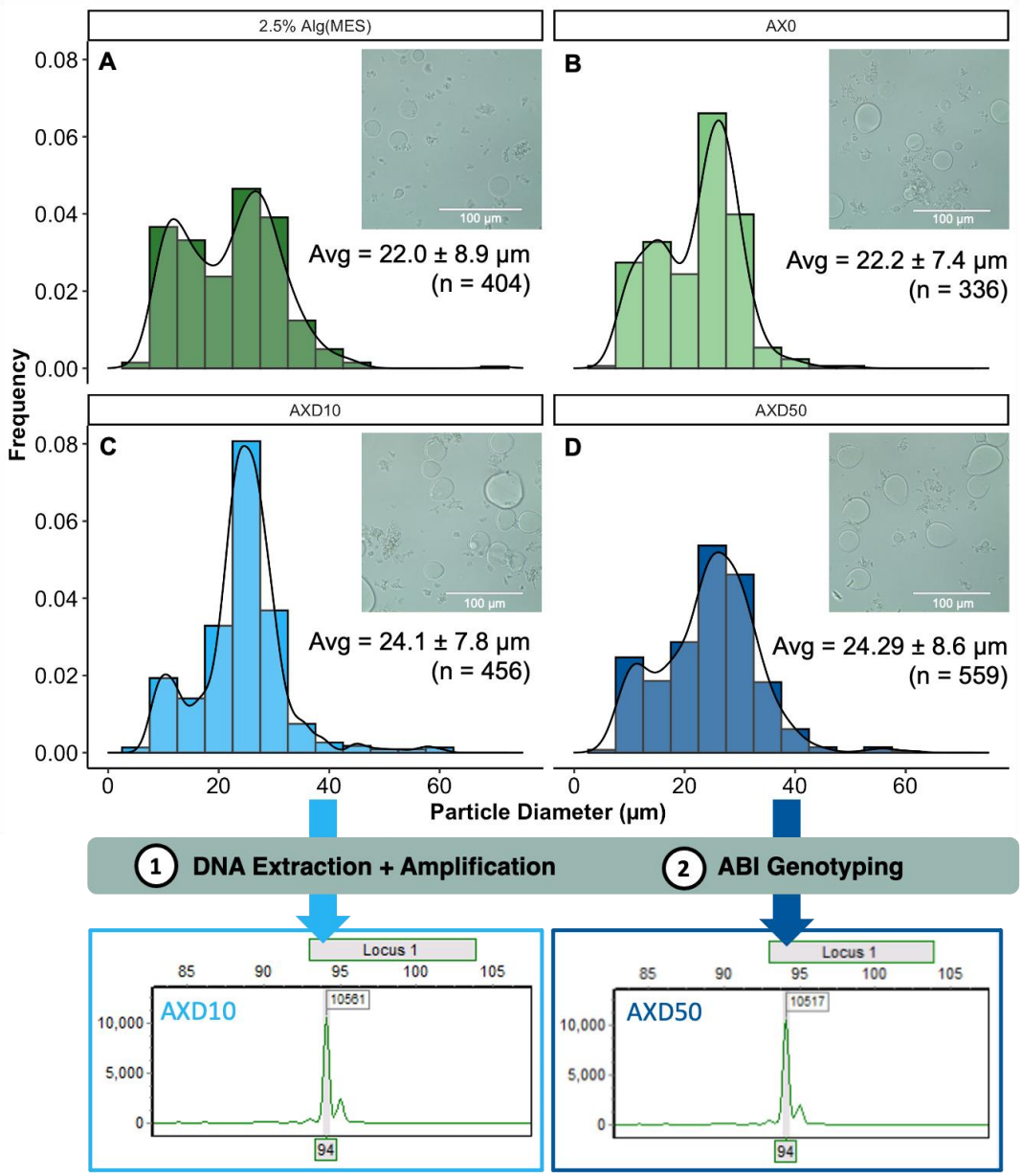

Figure 7: Microparticle (MP) size distribution of four different materials: 2.5% w/v alginate in MES buffer (A), AX0 (B), AXD10 (C) and AXD50 (D) electrosprayed with 0.5% v/v Tween 20 into a $CaCl_2$ bath. Inlet images show microscopic images of MPs visualized in brightfield mode at 40x magnification. Corresponding genotype of ssDNA extracted and amplified from AXD10 (E) and AXD50 (F) microparticles.

Therefore, by simply crosslinking alginate with ssDNA, the particles formed (our "WBCs") would be larger than those electrosprayed without DNA (our "RBCs") under the same conditions. Having two different cell mimetic types is not only important for the overall functionality of the blood material, but also the incorporation of viscoelastic RBCs is a critical feature to accurately simulate blood drop dynamics of spreading and splashing[63] in crime scene scenarios. Another important consideration in forensic blood simulants is the ability for materials to be processed in

a similar manner to blood evidence – specifically, the ability to extract, amplify and genotype the contained DNA. We investigated the overall functionality of the candidate WBCs and determined that following a typical blood processing procedure with an additional modification to break down the alginate material[41]), the crosslinked DNA could be extracted, amplified and produced an interpretable genotype similar to non-crosslinked controls (Figure 7). This is promising because it indicates that the crosslinked DNA still remains both functional and intact through the electrospraying process, generating viable WBC mimetics for forensic blood simulants.

4. Conclusions

This work explored the effect of covalent crosslinking between amine-terminated ssDNA and alginate and its role in generating MPs for forensic blood simulants. The covalent attachment of ssDNA to alginate provides more stable linkages and immobilization of the DNA within the hydrogels. The characterization of the alginate-DNA hydrogels demonstrated covalent crosslinking between alginate and ssDNA based on the detection of amide bonds in the highest DNA concentration material. The rheological assessments also showed that the AXD50 material had less frequency dependence in the tanδ, as well as dynamic gel characteristics in the high frequency range, unlike the other covalent crosslinked materials. This unique behaviour can be attributed to the higher number of crosslinks formed in the high DNA concentration material, where the flexible ssDNA allows for soft gel characteristics. Similarly, SEM revealed that the DNA crosslinked alginate hydrogels were more structured, with interconnected networks distinct from the alginate and DNA control materials. Finally, investigation into the molecular dynamics of the alginate and DNA crosslinking suggest that the binding of ssDNA primarily occurs from the primary amines at 5' and 3' ends, further supporting the development of 3D crosslinked networks in the reaction.

The attachment of DNA to the alginate backbone while maintaining functionality in MP form lends the material to such roles as mimetic WBCs in forensic blood simulants. The low G' characteristics of the covalent crosslinked Alg-DNA hydrogel is favourable for the development of MPs containing immobilized DNA, much like traditional WBCs in human blood. This work provides the baseline for the development of our alginate-based forensic blood simulant. Future works include characterizing these materials in the complex biological and physical processes that occur during evidence formation and degradation at the crime scene.

AUTHOR INFORMATION

Corresponding Author

Amanda Orr - *Environmental and Life Sciences Graduate Program (PhD), Trent University, 1600 West Bank Drive, Peterborough, ON, K9J 0G2*

orcid.org/0000-0002-2245-8448; Email: amandorr@trentu.ca

Authors

Paul Wilson - *Biology Department, Trent University, 1600 West Bank Drive, Peterborough, ON, K9J 0G2;* orcid.org/0000-0002-8176-0233

Theresa Stotesbury - *Faculty of Science, Forensic Science, Ontario Tech University, 2000 Simcoe Street North, Oshawa, ON, L1G 0C5;* orcid.org/0000-0001-6452-4389

FUNDING SOURCES

The author A.O is funded by the Natural Sciences and Engineering Research Council of Canada (NSERC) Doctoral Canada Graduate Scholarship. This work was also supported by NSERC Discovery Grant [Award Number RGPIN-2020-05816] to T.S; and NSERC Discovery Grant [Award Number RGPIN-2015-05637] to P.W.

NOTES

The authors declare no competing financial interest.

ACKNOWLEDGMENTS

Thank you to Ed Wilson of the Trent University Science Workshop for the construction of the aluminum plate used in the electrospray set up. Thank you to Dr. Ira Ebralidze from Ontario Tech Materials Characterization Facility for help with SEM imaging and to Nobelgen for access to the microscope for particle imaging.

ABBREVIATIONS

DNA, deoxyribonucleic acid; **ssDNA**, single stranded DNA; **RBCs**, red blood cells; **WBCs**, white blood cells; **MP**, microparticle; **N-DNA-N**, dual amine terminated ssDNA; **N-DNA**, single amine terminated ssDNA. **FTIR**, Fourier Transform infrared spectroscopy; **SEM**, scanning electron microscopy; **TGA**, thermogravimetric analysis. **CODIS**, Combined DNA Index System; **CATG**, calcium alginate tissue gels; **MES**, 2-(N-morpholino)ethanesulfonic acid; **EDC**, 1-ethyl-3-(3-

dimethylaminopropyl) carbodiimide•HCl; Sulfo-NHS, N-hydroxysuccimide; G', storage modulus; G" loss modulus.

REFERENCES

(1) Szekalska, M.; Puciłowska, A.; Szymańska, E.; Ciosek, P.; Winnicka, K. Alginate: Current Use and Future Perspectives in Pharmaceutical and Biomedical Applications. *Int. J. Polym. Sci.* 2016, *2016*, 1–17. DOI: 10.1155/2016/7697031.

(2) Mallakpour, S.; Azadi, E.; Hussain, C. M. State-of-the-Art of 3D Printing Technology of Alginate-Based Hydrogels—An Emerging Technique for Industrial Applications. *Adv. Colloid Interface Sci.* 2021, *293*, 102436. DOI: 10.1016/j.cis.2021.102436.

(3) Rinaudo, M. Biomaterials Based on a Natural Polysaccharide: Alginate. *TIP Rev. Espec. en Ciencias Químico-Biológicas* 2014, *17* (1), 92–96. DOI: 10.1016/S1405-888X(14)70322-5.

(4) Parreidt, T. S.; Müller, K.; Schmid, M. Alginate-Based Edible Films and Coatings for Food Packaging Applications. *Foods* 2018, *7* (10), 1–38. DOI: 10.3390/foods7100170.

(5) Lee, K. Y.; Mooney, D. J. Alginate: Properties and Biomedical Applications. *Prog. Polym. Sci.* 2012, *37* (1), 106–126. DOI: 10.1016/j.progpolymsci.2011.06.003.

(6) Neves, M. I.; Moroni, L.; Barrias, C. C. Modulating Alginate Hydrogels for Improved Biological Performance as Cellular 3D Microenvironments. *Front. Bioeng. Biotechnol.* 2020, *8* (June). DOI: 10.3389/fbioe.2020.00665.

(7) Gattás-Asfura, K. M.; Stabler, C. L. Chemoselective Cross-Linking and Functionalization of Alginate via Staudinger Ligation. *Biomacromolecules* 2009, *10* (11), 3122–3129. DOI: 10.1021/bm900789a.

(8) Kim, E.; Kim, M. H.; Song, J. H.; Kang, C.; Park, W. H. Dual Crosslinked Alginate Hydrogels by Riboflavin as Photoinitiator. *Int. J. Biol. Macromol.* 2020, *154*, 989–998. DOI: 10.1016/j.ijbiomac.2020.03.134.

(9) Bonino, C. A.; Samorezov, J. E.; Jeon, O.; Alsberg, E.; Khan, S. A. Real-Time in Situ Rheology of Alginate Hydrogel Photocrosslinking. *Soft Matter* 2011, *7* (24), 11510–11517. DOI: 10.1039/c1sm06109g.

(10) Samorezov, J. E.; Morlock, C. M.; Alsberg, E. Dual Ionic and Photo-Crosslinked Alginate Hydrogels for Micropatterned Spatial Control of Material Properties and Cell Behavior. *Bioconjug. Chem.* 2015, *26* (7), 1339–1347. DOI: 10.1021/acs.bioconjchem.5b00117.

(11) Moody, C. T.; Palvai, S.; Brudno, Y. Click Crossl-Linking Improves Retention and Targeting of Refillable Alginate Deposits. *Acta Biomater.* 2020, *112*, 112–121. DOI: 10.1016/j.actbio.2020.05.033.

(12) Augst, A. D.; Kong, H. J.; Mooney, D. J. Alginate Hydrogels as Biomaterials. *Macromol. Biosci.* 2006, *6* (8), 623–633. DOI: 10.1002/mabi.200600069.

(13) Cammarata, C. R.; Hughes, M. E.; Ofner III, C. M. Carbodiimide Induced Cross-Linking, Ligand Addition, and Degradation in Gelatin. *Mol Pharm* 2015, *12* (3), 783–793. DOI: 10.1021/mp5006118.

(14) Aguero, L.; Alpdagtas, S.; Ilhan, E.; Zaldivar-Silva, D.; Gunduz, O. Functional Role of Crosslinking in Alginate Scaffold for Drug Delivery and Tissue Engineering: A Review. *Eur. Polym. J.* 2021, *160* (September), 110807. DOI: 10.1016/j.eurpolymj.2021.110807.

(15) Sun, J.; Tan, H. Alginate-Based Biomaterials for Regenerative Medicine Applications.

Materials (Basel). 2013, *6* (4), 1285–1309. DOI: 10.3390/ma6041285.
(16) Devolder, R.; Kong, H. J. Hydrogels for in Vivo-like Three-Dimensional Cellular Studies. *WIREs Syst. Biol. Med.* 2012, *4* (4), 351–365. DOI: 10.1002/wsbm.1174.
(17) Basu, T.; Bhutani, U.; Majumdar, S. Cross-Linker-Free Sodium Alginate and Gelatin Hydrogels: A Multiscale Biomaterial Design Framework. *J. Mater. Chem. B* 2022, *10* (19), 3614–3623. DOI: 10.1039/d2tb00028h.
(18) Zhao, L.; Li, L.; Yang, G.; Wei, B.; Ma, Y.; Qu, F. Aptamer Functionalized DNA Hydrogels: Design, Applications and Kinetics. *Biosens. Bioelectron.* 2021, *194*, 113597. DOI: 10.1016/j.bios.2021.113597.
(19) Gačanin, J.; Synatschke, C. V.; Weil, T. Biomedical Applications of DNA-Based Hydrogels. *Adv. Funct. Mater.* 2020, *30* (4), 1–25. DOI: 10.1002/adfm.201906253.
(20) Murakami, Y.; Maeda, M. DNA-Responsive Hydrogels That Can Shrink or Swell. *Biomacromolecules* 2005, *6* (6), 2927–2929. DOI: 10.1021/bm0504330.
(21) Basu, S.; Pacelli, S.; Paul, A. Self-Healing DNA-Based Injectable Hydrogels with Reversible Covalent Linkages for Controlled Drug Delivery. *Acta Biomater.* 2020, *105*, 159–169. DOI: 10.1016/j.actbio.2020.01.021.
(22) Abune, L.; Davis, B.; Wang, Y. Aptamer-Functionalized Hydrogels: An Emerging Class of Biomaterials for Protein Delivery, Cell Capture, Regenerative Medicine, and Molecular Biosensing. *Wiley Interdiscip. Rev. Nanomedicine Nanobiotechnology* 2021, *13* (6), 1–25. DOI: 10.1002/wnan.1731.
(23) Li, W.; Wang, J.; Ren, J.; Qu, X. Endogenous Signalling Control of Cell Adhesion by Using Aptamer Functionalized Biocompatible Hydrogel. *Chem. Sci.* 2015, *6* (12), 6762–6768. DOI: 10.1039/c5sc02565f.
(24) Turner, D. A.; Baldwin, E.; Russell, K.; Wells, L. A. DNA-Crosslinked Alginate and Layered Microspheres to Modulate the Release of Encapsulated FITC-Dextran. *Eur. J. Pharm. Biopharm.* 2021, *158*, 313–322. DOI: 10.1016/j.ejpb.2020.11.016.
(25) Bush, J.; Hu, C. H.; Veneziano, R. Mechanical Properties of DNA Hydrogels: Towards Highly Programmable Biomaterials. *Appl. Sci.* 2021, *11* (4), 1–20. DOI: 10.3390/app11041885.
(26) Khajouei, S.; Ravan, H.; Ebrahimi, A. DNA Hydrogel-Empowered Biosensing. *Adv. Colloid Interface Sci.* 2019, *275*, 102060. DOI: 10.1016/j.cis.2019.102060.
(27) Li, C.; Chen, P.; Shao, Y.; Zhou, X.; Wu, Y.; Yang, Z.; Li, Z.; Weil, T.; Liu, D. A Writable Polypeptide-DNA Hydrogel with Rationally Designed Multi-Modification Sites. *Small* 2015, *11* (9–10), 1138–1143. DOI: 10.1002/smll.201401906.
(28) Wu, Y.; Li, C.; Boldt, F.; Wang, Y.; Kuan, S. L.; Tran, T. T.; Mikhalevich, V.; Förtsch, C.; Barth, H.; Yang, Z.; Liu, D.; Weil, T. Programmable Protein–DNA Hybrid Hydrogels for the Immobilization and Release of Functional Proteins. *Chem. Commun.* 2014, *50* (93), 14620–14622. DOI: 10.1039/c4cc07144a.
(29) Lu, C. H.; Guo, W.; Hu, Y.; Qi, X. J.; Willner, I. Multitriggered Shape-Memory Acrylamide-DNA Hydrogels. *J. Am. Chem. Soc.* 2015, *137* (50), 15723–15731. DOI: 10.1021/jacs.5b06510.
(30) Wang, C.; Fadeev, M.; Zhang, J.; Vázquez-González, M.; Davidson-Rozenfeld, G.; Tian, H.; Willner, I. Shape-Memory and Self-Healing Functions of DNA-Based Carboxymethyl Cellulose Hydrogels Driven by Chemical or Light Triggers. *Chem. Sci.* 2018, *9* (35), 7145–7152. DOI: 10.1039/c8sc02411a.

(31) Zhao, H.; Jiang, G.; Weng, J.; Ma, Q.; Zhang, H.; Ito, Y.; Liu, M. A Signal-Accumulating DNAzyme-Crosslinked Hydrogel for Colorimetric Sensing of Hydrogen Peroxide. *J. Mater. Chem. B* 2016, *4* (27), 4648–4651. DOI: 10.1039/c6tb00825a.
(32) Yang, H.; Liu, H.; Kang, H.; Tan, W. Engineering Target-Responsive Hydrogels Based on Aptamer-Target Interactions. *J. Am. Chem. Soc.* 2008, *130* (20), 6320–6321. DOI: 10.1021/ja801339w.
(33) Zhu, Z.; Wu, C.; Liu, H.; Zou, Y.; Zhang, X.; Kang, H.; Yang, C. J.; Tan, W. An Aptamer Cross-Linked Hydrogel as a Colorimetric Platform for Visual Detection. *Angew. Chemie* 2010, *122* (6), 1070–1074. DOI: 10.1002/ange.200905570.
(34) Pandey, R.; Lu, Y.; Osman, E.; Saxena, S.; Zhang, Z.; Qian, S.; Pollinzi, A.; Smieja, M.; Li, Y.; Soleymani, L.; Hoare, T. DNAzyme-Immobilizing Microgel Magnetic Beads Enable Rapid, Specific, Culture-Free, and Wash-Free Electrochemical Quantification of Bacteria in Untreated Urine. *ACS Sensors* 2022, *7* (4), 985–994. DOI: 10.1021/acssensors.1c02440.
(35) Li, J.; Zhang, Y.; Zhu, L.; Chen, K.; Li, X.; Xu, W. Smart Nucleic Acid Hydrogels with High Stimuli-Responsiveness in Biomedical Fields. *Int. J. Mol. Sci.* 2022, *23* (3), 1068. DOI: 10.3390/ijms23031068.
(36) Um, S. H.; Lee, J. B.; Park, N.; Kwon, S. Y.; Umbach, C. C.; Luo, D. Enzyme-Catalysed Assembly of DNA Hydrogel. *Nat. Mater.* 2006, *5* (10), 797–801. DOI: 10.1038/nmat1741.
(37) Gooch, J.; Daniel, B.; Parkin, M.; Frascione, N. Developing Aptasensors for Forensic Analysis. *TrAC - Trends Anal. Chem.* 2017, *94*, 150–160. DOI: 10.1016/j.trac.2017.07.019.
(38) Hai, J.; Wang, H.; Sun, P.; Li, T.; Lu, S.; Zhao, Y.; Wang, B. Smart Responsive Luminescent Aptamer-Functionalized Covalent Organic Framework Hydrogel for High-Resolution Visualization and Security Protection of Latent Fingerprints. *ACS Appl. Mater. Interfaces* 2019, *11* (47), 44664–44672. DOI: 10.1021/acsami.9b18251.
(39) Hammond, H. A.; Jin, L.; Zhong, Y.; Thomas Caskey, C.; Chakraborty, R. Evaluation of 13 Short Tandem Repeat Loci for Use in Personal Identification Applications. *Am. J. Hum. Genet.* 1994, *55* (1), 175–189.
(40) National Institute of Standards and Technology. *STRBase (SRD-130) - CSF1PO*. https://strbase.nist.gov/str_CSF1PO.htm.
(41) Orr, A.; Wilson, P.; Stotesbury, T. Calcium-Alginate Tissue Gels (CATG): Proof-of-Concept Biomaterial Development. *Forensic Sci. Int.* 2021, *329*, 111055. DOI: 10.1016/j.forsciint.2021.111055.
(42) Basu, S.; Alkiswani, A. R.; Pacelli, S.; Paul, A. Nucleic Acid-Based Dual Cross-Linked Hydrogels for in Situ Tissue Repair via Directional Stem Cell Migration. *ACS Appl. Mater. Interfaces* 2019, *11* (38), 34621–34633. DOI: 10.1021/acsami.9b10074.
(43) Zhou, J.; Rossi, J. Aptamers as Targeted Therapeutics: Current Potential and Challenges. *Nat Rev Drug Discov* 2017, *16* (3), 181–202. DOI: 10.1038/nrd.2016.199.
(44) Lin, D. C.; Yurke, B.; Langrana, N. A. Mechanical Properties of a Reversible, DNA-Crosslinked Polyacrylamide Hydrogel. *J. Biomech. Eng.* 2004, *126* (1), 104–110. DOI: 10.1115/1.1645529.
(45) Pan, W.; Wen, H.; Niu, L.; Su, C.; Liu, C.; Zhao, J.; Mao, C.; Liang, D. Effects of Chain Flexibility on the Properties of DNA Hydrogels. *Soft Matter* 2016, *12* (25), 5537–5541. DOI: 10.1039/c6sm00283h.
(46) Jiang, H.; Pan, V.; Vivek, S.; Weeks, E. R.; Ke, Y. Programmable DNA Hydrogels Assembled

from Multidomain DNA Strands. *ChemBioChem* 2016, *17* (12), 1156–1162. DOI: 10.1002/cbic.201500686.
(47) Ewoldt, R. H.; Johnston, M. T.; Caretta, L. M. *Experimental Challenges of Shear Rheology: How to Avoid Bad Data*; Springer, 2015. DOI: 10.1007/978-1-4939-2065-5_6.
(48) Goudoulas, T. B.; Pan, S.; Germann, N. Double-Stranded and Single-Stranded Well-Entangled DNA Solutions under LAOS: A Comprehensive Study. *Polymer (Guildf).* 2018, *140*, 240–254. DOI: 10.1016/j.polymer.2018.02.061.
(49) Gu, S.; Cheng, G.; Yang, T.; Ren, X.; Gao, G. Mechanical and Rheological Behavior of Hybrid Cross-Linked Polyacrylamide/Cationic Micelle Hydrogels. *Macromol. Mater. Eng.* 2017, *302*, 1–7. DOI: 10.1002/mame.201700402.
(50) Yesilyurt, V.; Webber, M. J.; Appel, E. A.; Godwin, C.; Langer, R.; Anderson, D. G. Injectable Self-Healing Glucose-Responsive Hydrogels with PH-Regulated Mechanical Properties. *Adv. Mater.* 2016, *28* (1), 86–91. DOI: 10.1002/adma.201502902.
(51) Besiri, I. N.; Goudoulas, T. B.; Germann, N. Impact of CaCl2 Concentration and in Situ Rheometric Setup Configuration on Fast Alginate–Ca 2+ Reaction. *Phys. Fluids* 2022, *34* (5), 053104. DOI: 10.1063/5.0090679.
(52) Huang, S.; Wang, J.; Zhang, Y.; Yu, Z.; Qi, C. Quaternized Carboxymethyl Chitosan-Based Silver Nanoparticles Hybrid: Microwave-Assisted Synthesis, Characterization and Antibacterial Activity. *Nanomaterials* 2016, *6* (6), 118. DOI: 10.3390/nano6060118.
(53) Di Foggia, M.; Taddei, P.; Torreggiani, A.; Dettin, M.; Tinti, A. Self-Assembling Peptides for Biomedical Applications: IR and Raman Spectroscopies for the Study of Secondary Structure Article. *Proteomics Res. J.* 2011, *2* (3), 231–272.
(54) Saarai, A.; Kasparkova, V.; Sedlacek, T.; Saha, P. On the Development and Characterisation of Crosslinked Sodium Alginate/Gelatine Hydrogels. *J. Mech. Behav. Biomed. Mater.* 2013, *18*, 152–166. DOI: 10.1016/j.jmbbm.2012.11.010.
(55) Wickramathilaka, M. P.; Tao, B. Y. Characterization of Covalent Crosslinking Strategies for Synthesizing DNA-Based Bioconjugates. *J. Biol. Eng.* 2019, *13* (1), 8–17. DOI: 10.1186/s13036-019-0191-2.
(56) Ayouch, I.; Barrak, I.; Kassab, Z.; El Achaby, M.; Barhoun, A.; Draoui, K. Impact of the Drying Process on the Efficiency of Alginate Beads for Cadmium Removal from Water: Kinetic, Isotherm and Thermodynamic Study. *Environ. Technol. Innov.* 2020, *20*, 101157. DOI: 10.1016/j.eti.2020.101157.
(57) Cesco, C. T.; Valente, A. J. M.; Paulino, A. T. Methylene Blue Release from Chitosan/Pectin and Chitosan/Dna Blend Hydrogels. *Pharmaceutics* 2021, *13* (6), 1–18. DOI: 10.3390/pharmaceutics13060842.
(58) Stotesbury, T.; Bruce, C.; Illes, M.; Hanley-Dafoe, R. Design Considerations for the Implementation of Artificial Fluids as Blood Substitutes for Educational and Training Use in the Forensic Sciences. *Forensic Sci. Policy Manag. An Int. J.* 2016, *7* (3–4), 81–86. DOI: 10.1080/19409044.2016.1218574.
(59) Stotesbury, T.; Illes, M.; Wilson, P.; Vreugdenhil, A. A Commentary on Synthetic Blood Substitute Research and Development. *J Bloodstain Pattern Anal.* 2015, *31* (2), 3–6.
(60) Morais, A. Í. S.; Vieira, E. G.; Afewerki, S.; Sousa, R. B.; Honorio, L. M. C.; Cambrussi, A. N. C. O.; Santos, J. A.; Bezerra, R. D. S.; Furtini, J. A. O.; Silva-Filho, E. C.; Webster, T. J.; Lobo, A. O. Fabrication of Polymeric Microparticles by Electrospray: The Impact of Experimental

Parameters. *J. Funct. Biomater.* 2020, *11* (1), 4. DOI: 10.3390/jfb11010004.
(61) Perez-Masia, R.; Lagaron, J. M.; Lopez-Rubio, A. Surfactant-Aided Electrospraying of Low Molecular Weight Carbohydrate Polymers from Aqueous Solutions. *Carbohydr. Polym.* 2014, *101* (1), 249–255. DOI: 10.1016/j.carbpol.2013.09.032.
(62) Alallam, B.; Altahhan, S.; Taher, M.; Mohd Nasir, M. H.; Doolaanea, A. A. Electrosprayed Alginate Nanoparticles as Crispr Plasmid Dna Delivery Carrier: Preparation, Optimization, and Characterization. *Pharmaceuticals* 2020, *13* (8), 1–29. DOI: 10.3390/ph13080158.
(63) Yokoyama, Y.; Tanaka, A.; Tagawa, Y. Droplet Impact of Blood and Blood Simulants on a Solid Surface: Effect of the Deformability of Red Blood Cells and the Elasticity of Plasma. *Forensic Sci. Int.* 2022, *331*, 111138. DOI: 10.1016/j.forsciint.2021.111138.